IEEE Access
Multidisciplinary | Rapid Review | Open Access Journal

Received 6 July 2022, accepted 18 July 2022, date of publication 28 July 2022, date of current version 3 August 2022.

Digital Object Identifier 10.1109/ACCESS.2022.3194532

RESEARCH ARTICLE

Fast-Update Iterative Learning Control for Performance Enhancement With Application to Motion Systems

YULIN WANG[1,2] AND TESHENG HSIAO[2], (Member, IEEE)
[1]College of Mechanical Engineering, Guangdong Ocean University, Zhanjiang 524088, China
[2]Institute of Electrical and Control Engineering, National Yang Ming Chiao Tung University, Hsinchu 30010, Taiwan

Corresponding author: Tesheng Hsiao (tshsiao@cn.nctu.edu.tw)

ABSTRACT Iterative learning control (ILC) algorithms are typically used to improve the performance of repetitive processes. Numerous successful applications of ILC, such as computer numerical control (CNC) machining processes, robot manipulation, and lithography processes, have been reported. However, ILC often exhibits less than satisfactory performance since the control unit operates at a limited sampling rate in consideration of cost. In this study, the multiloop, multirate structure of servo motor control systems is taken advantage of and a fast-update multirate ILC (FILC) scheme is proposed for high-accuracy trajectory tracking, where compensation is updated at a rate faster than that of the original position loop without the need for redesigning the feedback controller. The key difficulty related to the design of the FILC lies in the extremely complex and time-varying dynamics inherent in multirate systems. To address this problem, a novel equivalent single-rate parametric model description of the multirate system is derived, which enables the use of the efficient norm optimal ILC algorithm. Consequently, a computationally efficient FILC is obtained to improve the performance. Subsequently, the proposed FILC is applied to the position control of the CNC motion stage. Simulation and experimental results are used to verify the effectiveness of the proposed method.

INDEX TERMS Iterative learning control, multirate system, norm optimal, linear periodic time varying, precise motion control.

I. INTRODUCTION

Due to the rapid development and strength of digital technologies, almost all control laws are currently implemented in digital forms, which together with continuous-time plants constitute the sampled-data control systems. In sampled-data control systems, the sampling rate should be much higher than the control bandwidth to diminish the effects of discretization [1]. Unfortunately, this requirement may not always be satisfied in some advanced applications, partly because of the ever demanding needs for higher performance and bandwidth and partly because of cost considerations. Consequently, the control system is susceptible to disturbances beyond the Nyquist frequency and unmeasurable ripples or oscillations between samples, especially for systems with nonminimum phase zeros, leading to performance deterioration [2].

Extensive research has been dedicated to the performance enhancement of sampled-data control systems in the form of either feedback or feedforward compensation, while the multirate configuration is one of the most popular techniques for reaching a compromise between performance and cost [2]–[5]. The zero-phase error tracking control (ZPETC) method was applied in [4] to approximate the system inversion and obtain fast-update multirate feedforward compensation without changing the existing feedback control architecture; however, its performance was limited because of the inaccuracy of the inversion approximation. Alternatively, preactuated multirate feedforward control was proposed in [2], and the stable inversion method was used to process

The associate editor coordinating the review of this manuscript and approving it for publication was Zhong Wu.

the discretization zeros and intrinsic zeros with the aim of balancing on sample and intersample behavior. In [5], two decomposed subsystems were obtained to enhance continuous-time performance, and a multirate inversion was then applied. In [3] and [6], a multirate disturbance observer (DOB) was designed that suppresses disturbances beyond the Nyquist frequency. It is worth noting that the above methods have a common feature: the control inputs from the feedforward controller or DOB are fast updated, which is understandable because high-rate signals contain rich information that is useful for performance improvement.

Among all the approaches for control performance enhancement, ILC is particularly attractive owing to its effectiveness and simple structure. There are many original works and surveys on ILC [7]–[11]. ILC is a digital feedforward control approach used to improve the performance of the current trial based on the results of the previous trial during repetitive operations. Identical initial conditions are utilized for each trial. Such operations are common in manufacturing, assembling and data storage devices. Examples include injection molds [12], robotic manipulator pick-and-place movement [13]–[15], precision positioning of the wafer stage [16], hard disk drive servo systems [17], and CNC machine tools [18].

Compared with well-designed feedback control and feedforward control, ILC has unique advantages. For example, all feedback controllers, including the state-of-the-art intelligent algorithm-based feedback controllers [19], respond to reference changes and disturbances with inherent delays and transients. In contrast, noncausal ILC algorithms can be designed to preemptively target future reference commands and disturbances in the time domain. Feedforward control can also improve the phase lag in reference tracking control but cannot suppress disturbances. In contrast, ILC can suppress repetitive disturbances without requiring precise information about the system or disturbances. This is because the ILC output is the result of input errors with rich information from previous trials. In addition, feedback control and ILC are commonly used in combination to suppress nonrepetitive and repetitive disturbances, respectively. The most recent developments of ILC include trial-varying trajectory following spatial ILC, learning basis functions, and data driven methods for performance enhancement [20]–[25].

The objective of our work is to apply ILC to improve the performance of sampled-data systems that perform repetitive tasks in the multirate framework. In [26] and [27], a pseudo downsampled technique was derived for a P-type multirate ILC; however, this approach was limited by the fact that reducing the sampling rate of the error input may result in the loss of some frequency information. Alternatively, a multirate ILC method aiming to suppress intersample oscillation was proposed in [28], in which fast output measurements were obtained for an ILC with a slow-rate design. Due to the lack of a parameterized multirate system model, an additional lifting step was taken, which involved the demanding computation of a large-sized matrix convolution and thus restricted this approach to only short-length tasks (less than 10^3 samples).This inefficiency can be considerably mitigated by multirate fast-updated state tracking ILC reported in [29], Similarly, a patent application for multirate fast-update output tracking ILC developed in [30]. Still, the error convergence is slow because they are both PD-type learning designs, instead of the model-based learning, which has a faster error convergence rate. The key difficulty in designing a model-based multirate ILC is the parametric model for the multirate system description. Hence, a novel time-varying parametric model will be presented in this paper.

Compared with information-rich fast-update multirate ILC (FILC), slow-update single-rate ILC (SILC) is generally suboptimal. Motivated by the potential performance gains of multirate feedforward control in the literature [2], [3], [28], [29], an FILC scheme is proposed in this paper under the assumption that a fast-rate system output is available. Moreover, the proposed scheme overcomes the major challenge common in FILC methods, i.e., establishing a parametric multirate system description, and efficiently uses the model-based norm optimal algorithm to make it feasible for practical applications. Then, we demonstrate through experiments that the proposed FILC scheme can be seamlessly integrated into the conventional multiloop, multirate servo motor control system with minimum hardware modification to improve the trajectory tracking performance.

Therefore, the essential contribution of this paper is the development of a framework that exploits FILC to enhance the performance of sampled-data systems. More precisely, the following subcontributions are identified:

(C1) The FILC framework is designed based on an efficient norm optimal algorithm.

(C2) The time-varying parametric multirate system is described.

(C3) The FILC framework is applied for the position control of a ball-screw-driven CNC machine tool motion stage and validated through simulations and experiments.

The organization of this paper is as follows: In Section II, the mathematic preliminaries and problem formulation are presented, and the efficient norm optimal ILC method combined with feedback control for time-varying systems is introduced. A parametric multirate system description is presented in Section III. In Section IV, the advantages of the proposed FILC are demonstrated via simulations and experiments. The conclusions are presented in Section V.

II. PRELIMINARIES AND PROBLEM FORMULATION

In the first subsection, we present the notations and conventions adopted in this paper. In the second subsection, the standard ILC for general sampled-data systems, which operates at a single slow rate and is abbreviated as SILC, is introduced. In addition, the shortcomings of SILC are discussed. The third subsection introduces FILC, including its advantages over SILC and its challenges in design and implementation, thereby constituting contribution C1. Next,

we illustrate the strategy to overcome the challenges in Section III.

A. NOTATION

We introduce the notations and conventions that will be followed throughout this paper. The index of a discrete-time signal and a continuous-time signal are surrounded by brackets and parentheses, respectively. For example, $y(t)$ denotes the value of a continuous-time signal at time t, whereas $y[k]$ denotes the value of a discrete-time signal at the k^{th} sample.

For discrete-time signals, z is used either as a time advanced operator in the time domain or the complex variable of the z-transform. The exact meaning of z will be clear from the context. For example, $zy[k] = y[k+1]$ for any discrete-time signal $y[k]$, while $P_d(z)$ denotes the transfer function of a discrete-time linear time-invariant (LTI) system.

In multirate ILC systems, repetitive tasks are considered, where each run of the task is called a trial. In addition, discrete-time signals and systems are sampled or operated with different sampling rates. Hence, we use the subscript to denote the trial of the signal and the superscript l or h to denote a signal or system sampled or operated with a low or high rate, respectively. For example, $y_j^l[k]$ represents the value of signal y, which is sampled at a low rate at the k^{th} sample of the j^{th} trial. If the sampling rate is irrelevant, the superscript can be omitted. Furthermore, suppose that the length of each trial is N. We can stack the N-point signal into a vector and use an underline to denote the vector form, that is, $\underline{y}_j^l = \left[y_j^l[0]\,, y_j^l[1], \cdots, y_j^l[N-1]\right]^T$.

The state space form of a discrete-time transfer function $P_d(z)$is denoted by

$$P_d\,(A,B,C,D) = \begin{cases} x[k+1] = Ax[k] + Bu[k] \\ y[k] = Cx[k] + Du[k]. \end{cases} \tag{1}$$

and$P_d(z) = C(zI - A)^{-1}B + D$.

Consider a discrete-time, linear time-varying (LTV), causal system, described in the state space form:

$$P_d\,(A[k], B[k], C[k], D[k]) = \begin{cases} x[k+1] = A[k]x[k] + B[k]u[k] \\ y[k] = C[k]x[k] + D[k]u[k]. \end{cases} \tag{2}$$

The input-output relation of $P_d\,(A[k], B[k], C[k], D[k])$ can be expressed in lifted form as

$$\underline{y}_j = \underbrace{\begin{bmatrix} D[0] & 0 & \cdots & 0 \\ h[1,0] & D[1] & \cdots & 0 \\ \vdots & \vdots & \ddots & \vdots \\ h[N-1,0] & h[N-1,1] & \cdots & D[N-1] \end{bmatrix}}_{\underline{P}_d} \underline{u}_j. \tag{3}$$

where $\underline{y}_j = (y_j[0], y_j[1], \cdots y_j[N-1])^T$ is the output and $\underline{u}_j = (u_j[0], u_j[1], \cdots u_j[N-1])^T$is the input. In addition, $h[k,i] = C[k]\Phi(k, i+1)B[i]$, where $\Phi(k, i+1) = A[k-1]A[k-2]\cdots A[i+1]$ is the state transition matrix of the LTV system. When the plant is time invariant,$\underline{P}_d$ is a Toeplitz matrix. The underline indicates the corresponding lifted matrix form.

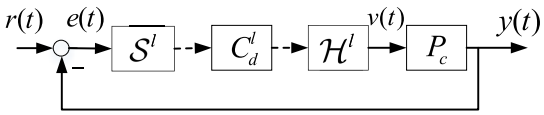

FIGURE 1. Sample-data control setup.

When a sampled-data control system is represented by a block diagram, we use solid, dashed, and dash-dotted lines for continuous-time signals, slow-rate discrete-time signals, and fast-rate discrete-time signals, respectively.

Let $\|\underline{x}\|_M^2 := \underline{x}^T M \underline{x}$, where $\underline{x} \in \mathbb{R}^n$ and $M \in \mathbb{R}^{n\times n}$. M is positive definite ($M \succ 0$) iff $\underline{x}^T M \underline{x} > 0, \forall \underline{x} \neq \underline{0}$ and positive semidefinite ($M \succeq 0$) if $\underline{x}^T M \underline{x} \geq 0, \forall \underline{x}$.

B. NORM OPTIMAL ILC FOR SAMPLED-DATA SYSTEMS

Consider the single-input, single-output sampled-data control system shown in Fig. 1, with reference trajectory $r(t)$, which is known in advance, output $y(t)$, control input $v(t)$, sampler $\mathcal{S}^l$, digital controller C_d^l, and the zero-order-hold (ZOH) $\mathcal{H}^l$. The continuous-time LTI plant P_c is given by:

$$\dot{x}(t) = A_c x(t) + B_c u(t). \tag{4a}$$
$$y(t) = C_c x(t). \tag{4b}$$

The discretized plant P_d^l, by means of the ZOH $\mathcal{H}^l$, and the sampler $\mathcal{S}^l$ with sampling rate $f^l = 1/\delta$ Hz, is given by $P_d^l = \mathcal{S}^l P_c \mathcal{H}^l$ with state space form:

$$x^l[k+1] = A_d^l x^l[k] + B_d^l u[k]. \tag{5a}$$
$$y^l[k] = C_d x^l[k]. \tag{5b}$$

with

$$A_d^l = e^{A_c\delta}, B_d^l = \int_0^\delta e^{A_c\tau} B_c d\tau, C_d = C_c. \tag{6}$$

Suppose that a digital controller with sampling time δ is designed to track a finite-length reference trajectory $r^l[k]$ for $k = 0, 1, \ldots N-1$. In addition, the controller should consider the model uncertainties of the plant and the stability of the feedback system. Based on the complexity of the control law, the computational power of the controller hardware, and the desired bandwidth of the system, the sampling time is chosen. Hence, modifying the feedback controller C_d^l takes considerable time and effort and is not considered in many practical applications. Instead, an add-on feedforward compensation such as ILC is preferred for performance enhancement.

The standard ILC operates at a single slow rate (the same rate as C_d^l) and introduces a feedforward control input u_j^l into the control system, as shown in Fig. 2. Let the tracking error of the $(j+1)^{th}$ trial be $e_{j+1}^l = r^l - y_{j+1}^l$. One common ILC design method is to minimize the performance criterion in Definition 1 based on the control input and error of the

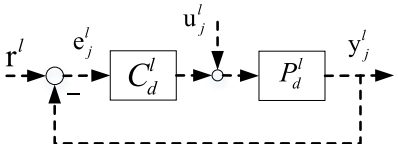

FIGURE 2. Standard (i.e. slow-update single-rate) ILC (SILC) structure.

previous trial, that is, $(\underline{u}_j^l, \underline{e}_j^l)$. This is called norm optimal ILC, the stability and convergence analysis can be guaranteed [7], [13], [14].

Definition 1 [Performance Criterion]: A standard performance criterion for the norm optimal ILC is given by

$$J(\underline{u}_{j+1}, \underline{e}_{j+1}) = \|\underline{e}_{j+1}\|^2_{W_q} + \|\underline{u}_{j+1} - \underline{u}_j\|^2_{W_r} + \|\underline{u}_{j+1}\|^2_{W_s}. \quad (7)$$

The weighting matrices $W_q \succ 0, W_r \succeq 0, W_s \succeq 0$ are used to penalize $\underline{e}_{j+1}$, $\underline{u}_{j+1} - \underline{u}_j$ and $\underline{u}_{j+1}$ respectively. The smaller W_r is, the larger $\underline{u}_{j+1} - \underline{u}_j$ is, which means that the ILC output is more sensitive to the error information in the previous trial; hence, the ILC is more sensitive to nonrepetitive disturbances. Additionally, a common method to improve robust monotonic convergence is to increase W_s; however, this comes at a slower error convergence rate [31]. Therefore, the combination of the weighting matrices is a trade-off between robustness and performance.

The weighting matrices are generally chosen as $W_q = w_q I_N$, $W_r = w_r I_N$ and $W_s = w_s I_N$, where I_N is the $N \times N$ identity matrix, and $w_q > 0, w_r, w_s \geq 0$.

The ILC input u_j^l in Fig. 2 can be computed by minimizing the cost function as follows:

$$\underline{u}_{j+1}^l = \arg\min J(\underline{u}_{j+1}^l, \underline{e}_{j+1}^l). \quad (8)$$

where the optimal solution of (8) is given in [14] and presented in Theorem 2. The proof can be found in [14] and is omitted here.

Theorem 2 [Solution of the Norm Optimal ILC]: Let $\underline{S} = (I_N + \underline{P}_d^l \underline{C}_d^l)^{-1}$ be the sensitivity function of the system in Fig. 2, where $\underline{P}_d^l$ and $\underline{C}_d^l$ are the lifted forms (3) of the plant and controller, respectively. We define $\underline{S}_u = \underline{S}\underline{P}_d^l$, which is the convolution matrix from $\underline{u}_j^l$ to $\underline{y}_j^l$, as in (3). Then, given $\underline{u}_j^l$ and $\underline{e}_j^l$, the norm optimal ILC update law is

$$\underline{u}_{j+1}^l = \underline{L}_u \underline{u}_j^l + \underline{L}_{ej}^{\ l}. \quad (9)$$

where

$$\underline{L}_u = (\underline{S}_u^T W_q \underline{S}_u + W_s + W_r)^{-1}(\underline{S}_u^T W_q \underline{S}_u + W_r). \quad (10)$$

$$\underline{L}_e = (\underline{S}_u s^T W_q \underline{S}_u + W_s + W_r)^{-1} \underline{S}_u^T W_q. \quad (11)$$

Note that the control law (9) involves inversion and multiplication of the $N \times N$ matrices, where N is the length of the task. As N increases, computational effort becomes increasingly demanding. This situation becomes much more severe when a high sampling rate is adopted. Therefore, Equation (9) is restricted to short-length tasks.

To overcome this problem, Zundert *et al.* [32] proposed a computationally efficient solution to the norm optimal ILC, which is presented in Theorem A1 in the *Appendix*. The proof of Theorem A1 can be found in [32].

The efficient norm optimal ILC in Theorem A1 significantly reduces the computation load. Moreover, it allows time-varying and noncausal computation, which forms the basis of this paper.

The results above are associated with a single rate. The plant in (4) needs to be discretized at a higher sampling rate to obtain a multirate scheme in the following subsection. Thus, the relationship between the discretized systems with different sampling rates is illustrated in Lemma 3.

Lemma 3: Let P_d^h be the discretized model of P_c in Fig. 1 with respect to a high sampling rate $f^h = F/\delta = Ff^l$, where $F \in \mathbb{N}$ is the multirate ratio, that is, $P_d^h = \mathcal{S}^h P_c \mathcal{H}^h$ with state space form

$$x^h[n+1] = A_d^h x^h[n] + B_d^h u^h[n]. \quad (12a)$$

$$y^h[n] = C_d x^h[n]. \quad (12b)$$

where

$$A_d^h = e^{A_c \delta/F}, B_d^h = \int_0^{\delta/F} e^{A_c \tau} B_c d\tau, C_d = C_c. \quad (13)$$

Then,

$$A_d^l = (A_d^h)^F$$
$$B_d^l = (A_d^h)^{F-1} B_d^h + (A_d^h)^{F-2} B_d^h + \cdots + B_d^h. \quad (14)$$

Proof: Comparing (13) with (6) and

$$A_d^l = (e^{A_c \delta/F})^F. \quad (15)$$

$$B_d^l = \int_0^{\delta/F} e^{A_c \tau} B_c d\tau + \int_{\delta/F}^{2\delta/F} e^{A_c \tau} B_c d\tau + \cdots + \int_{(F-1)\delta/F}^{\delta} e^{A_c \tau} B_c d\tau. \quad (16)$$

yields (14)

Note that from Lemma 3, we can directly obtain P_d^l from P_d^h.

C. FAST-UPDATE MULTIRATE ILC STRUCTURE

The SILC scheme in Fig. 2 can effectively suppress tracking errors provided that the desired bandwidth of the closed-loop system is much lower than the Nyquist frequency. However, as a higher and higher bandwidth is needed to meet increasingly stringent performance requirements, the sampled-data system may suffer from high-frequency distortion and aliasing of disturbances beyond the Nyquist frequency. In such a case, it is desirable to use a higher sampling rate. However, deploying a higher sampling rate usually requires redesigning the digital feedback controller and more demanding computational power, resulting in higher costs. Fortunately, the multirate architecture can strike a balance between the cost and performance. Additionally, the servo motor control system has an inherent multiloop and multirate structure, as presented in Section IV.A, consisting of the innermost current loop with the highest rate, the

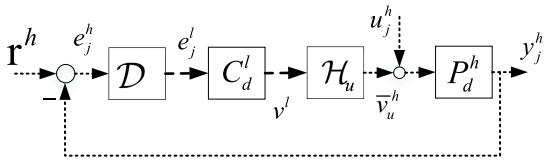

FIGURE 3. Fast-update multirate ILC (FILC) structure.

middle velocity loop with the medium rate, and the outermost position loop with the lowest rate. In the existing literature, ILC was only used to improve the performance within the position loop in a single-rate configuration without taking full advantage of the multirate scheme of the servo motor control system.

Based on these facts, we propose a fast-update multirate ILC (FILC) framework, as shown in Fig. 3, which minimizes the cost function in Definition 1 with a fast sampling rate:

$$\underline{u}_{j+1}^h = \arg\min J(\underline{u}_{j+1}^h, \underline{e}_{j+1}^h). \tag{17}$$

The downsampler $\mathcal{D}$ in Fig. 3 is used to select an integer multiple of $e_{j+1}^h[k]$ as $e_{j+1}^l[k]$, i.e.,

$$e_{j+1}^l[k] = e_{j+1}^h[Fk]. \tag{18}$$

Multirate holder $\mathcal{H}_u = \mathcal{H}_{zoh}\mathcal{U}$ is an up-sampler followed by a zero-order hold (ZOH), which is defined as follows:

$$\mathcal{H}_{zoh} = \sum_{i=0}^{F-1} z^{-i}. \tag{19}$$

$\mathcal{U} : x[k] \to x_u[k]$, and

$$x_u[k] = \begin{cases} x[k/F], & k = 0,\ F,\ 2F \cdots \\ 0, & \text{otherwise.} \end{cases} \tag{20}$$

From Fig. 3, we can see that the feedback controller C_d^l remains unaltered, and therefore, there is no need to redesign it. Instead, performance enhancement is attained by providing fast-update feedforward compensation based on the norm optimal ILC in (17). In addition, when we apply the proposed FILC to tracking control of the X-Z motion stage in Section IV, it is clear that the ILC compensation u_j^h is injected into the velocity loop, which operates at a higher sampling rate. Consequently, the changes in hardware are minimal when implementing the proposed FILC method.

Unfortunately, Theorem A1 cannot be directly applied to solve the norm optimal ILC problem in (17) because of the multirate structure shown in Fig. 3. In the next section, we derive a parametric multirate system description for the system in Fig. 3, which turns out to be a linear periodically time-varying (LPTV) system. Thus, (17) is tractable by applying Theorem A1 and the parametric multirate system description.

III. PARAMETRIC MULTIRATE SYSTEM DESCRIPTION

In this section, a novel parametric model for the multirate system, which forms contribution C2, is presented. In Section III-A, the standard ILC system described in Fig. 2 is modeled for comparison. In Section III-B, the time-varying feature of the multirate system is presented. An equivalent single fast rate is used to describe the multirate control system, as shown in Fig. 3. Then, based on these modeling methods and previous results, SILC and FILC are implemented in Section IV.

A. STATE SPACE DESCRIPTION FOR SILC

The SILC structure is a single-rate system, as shown in Fig. 2, and is described by the state space model in Lemma 4.

Lemma 4 [Parametric Description of SILC]: Let the LTI discrete-time plant P_d^l and the digital controller C_d^l in Fig. 2 be described in state space form as

$$P_d^l \left(A_p^l, B_p^l, C_p^l, 0\right) \text{ and } C_d^l \left(A_c^l, B_c^l, C_c^l, D_c^l\right). \tag{21}$$

Then, the state space description of the relationship $u_j^l[k] \to y_j^l[k]$ is as follows:

$$J_S(A, B, C, 0). \tag{22}$$

where $A = \begin{bmatrix} A_c^l & -B_c^l C_p^l \\ B_p^l C_c^l & A_p^l - B_p^l D_c^l C_p^l \end{bmatrix}$, $B = \begin{bmatrix} 0 \\ B_p^l \end{bmatrix}$, $C = \begin{bmatrix} 0 & C_p^l \end{bmatrix}$.

Proof: To find the relation from $u_j^l[k]$ to $y_j^l[k]$, the reference input r^l is omitted here. As shown in Fig. 2, the successive substitution of the state update and output equations of the subsystems yields the system representation $u_j^l[k] \to y_j^l[k]$ above.

B. STATE SPACE DESCRIPTION FOR FILC

The multirate system is illustrated in Fig. 3. A parametric description of the input-output mapping from $u_j^h[k]$ to $y_j^h[k]$ is required to solve the norm optimal ILC problem. However, the derivation is challenging because the mapping is time-varying owing to its multirate nature. To obtain the desired parametric description, we convert the multirate system into an equivalent fast-rate system in the sense that the input-output relation is reserved.

The holding selector is defined as a downsampler followed by a multirate holder, that is, $\mathcal{H}_u\mathcal{D}$. Note that both the input and output of the holding selector are fast-rate signals. Let $\bar{e}_j^h[k] = \mathcal{H}_u\mathcal{D}e_j^h[k]$. Then, the holding selector has the following time-varying state space representation:

$$x_s^h[k+1] = s[k]x_s^h[k] + (1 - s[k])\, e_j^h[k]. \tag{23a}$$

$$\bar{e}_j^h[k] = s[k]x_s^h[k] + (1 - s[k])\, e_j^h[k]. \tag{23b}$$

where $s[k] = \begin{cases} 0 \text{ if } k = \alpha F,\ \alpha \in \mathbb{Z} \\ 1 \quad \text{otherwise} \end{cases}$.

For the sake of convenience, we take $F = 2$ as an example and illustrate the operation of the holding selector in Table. 1, in which the correspondence of sample indices between the slow-rate signals and the fast-rate counterparts is listed. The entries in the same column in Table 1 correspond to the same time instance. Recall that $e_j^l[n]$=$e_j^h[Fn]$. From Table 1, we can

TABLE 1. Relation between the input and output of the system shown in Fig. 3.

k	0	1	2	3	4	5	...
n	0	–	1	–	2	–	...
$e_j^h[k]$	$e_j^h[0]$	$e_j^h[1]$	$e_j^h[2]$	$e_j^h[3]$	$e_j^h[4]$	$e_j^h[5]$	...
$e_j^l[n]$	$e_j^l[0]$	–	$e_j^l[1]$	–	$e_j^l[2]$	–	...
$\bar{e}_j^h[k]$	$e_j^h[0]$	$e_j^h[0]$	$e_j^h[2]$	$e_j^h[2]$	$e_j^h[4]$	$e_j^h[4]$	...
$v^l[n]$	$v^l[0]$	–	$v^l[1]$	–	$v^l[2]$	–	...
$v_u^h[k]$	$v_u^h[0]$	$v_u^h[0]$	$v_u^h[2]$	$v_u^h[2]$	$v_u^h[4]$	$v_u^h[4]$	...

In this table, k denotes the fast sample index, n denotes the slow sample index and '–' denotes a holding.

see that $\bar{e}_j^h[k]$ contains exactly the same information as $e_j^l[n]$. In other words, they correspond to identical continuous-time signals when converted through ZOH.

Next, we consider the slow-rate digital controller represented in the following state space form:

$$x_c^l[n+1] = A_c^l x_c^l[n] + B_c^l e_j^l[n]. \tag{24a}$$

$$v^l[n] = C_c^l x_c^l[n] + D_c^l e_j^l[n]. \tag{24b}$$

If we replace $e_j^l[n]$ in (24a) and (24b) with $\bar{e}_j^h[k]$ and replace $v^l[n]$ in (24b) with its equivalent fast-rate counterpart $\bar{v}_u^h = \mathcal{H}_u v^l$, that is, v^l and $\bar{v}_u^h$ are identical once they are converted to continuous-time signals by ZOH, the input-output relation of the controller does not change except that the sampling rate is increased by a factor of F. Given $\bar{e}_j^h[k]$ and $\bar{v}_u^h[k]$ as the input and output of the controller, respectively, the corresponding fast-rate state space representation of the controller for $F = 2$ is as follows:

$$\begin{aligned} x_c^h[0] &= 0 & x_c^h[1] &= x_c^h[0] \\ x_c^h[2] &= A_c^l x_c^h[1] + B_c^l \bar{e}_j^h[1] & x_c^h[3] &= x_c^h[2] \\ x_c^h[4] &= A_c^l x_c^h[3] + B_c^l \bar{e}_j^h[3] & x_c^h[5] &= x_c^h[4] \cdots \end{aligned} \quad . \tag{25}$$

Using the result above, the output $\bar{v}_u^h[k]$ of the controller yields

$$\begin{aligned} \bar{v}_u^h[2k] &= C_c^l x_c^h[2k] + D_c^l \bar{e}_j^h[2k] \\ \bar{v}_u^h[2k+1] &= \bar{v}_u^h[2k] = C_c^l x_c^h[2k+1] + D_c^l \bar{e}_j^h[2k+1]. \end{aligned} \tag{26}$$

where $k = 0, 1, 2 \cdots$.

From the above derivation, the equivalent fast-rate state space representation of the controller is given as

$$\hat{C}_c(\hat{A}_c^h[k], \hat{B}_c^h[k], C_c^l, D_c^l). \tag{27}$$

where

$$\hat{A}_c^h[k] = \begin{cases} A_c^l & \text{if } k = \alpha F - 1,\ \alpha \in \mathbb{N} \\ I & \text{otherwise} \end{cases} \tag{28}$$

$$\hat{B}_c^h[k] = \begin{cases} B_c^l & \text{if } k = \alpha F - 1,\ \alpha \in \mathbb{N} \\ 0 & \text{otherwise} \end{cases} \tag{29}$$

Let $P_d\left(A_p^h, B_p^h, C_p^h, 0\right)$ be the state space representation of a discrete-time plant sampled by the fast rate. Subsequently,

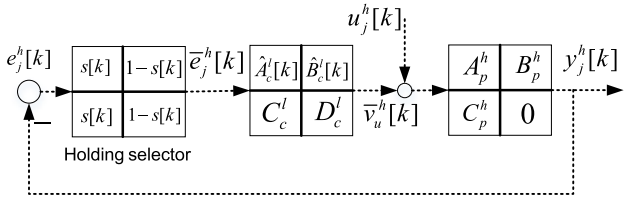

FIGURE 4. Equivalent time-domain multirate system structure.

we convert all slow-rate signals in Fig. 3 into their equivalent fast-rate counterparts and derive the equivalent fast-rate state space form of each block. Hence, the multirate system in Fig. 3 can be transformed into the fast-rate system shown in Fig. 4 with equivalent input and output signals. The reference is omitted in Fig. 4 for simplicity since we need the model from $u_j^h[k]$ to $y_j^h[k]$. Consequently, we obtain the following parametric description of the proposed FILC system.

Theorem 5 [Parametric Description of FILC]: As shown in Fig. 4, the state space description of the relationship $u_{j+1}^h[k] \to y_{j+1}^h[k]$ is given as follows:

$$J_F\left(A[k], B, C, 0\right). \tag{30}$$

where

$$A[k] = \begin{bmatrix} s[k] & 0 & -(1-s[k])\, C_p^h \\ \hat{B}_c^h[k]s[k] & \hat{A}_c^h[k] & -\left(\hat{B}_c^h[k](1-s[k])\right) C_p^h \\ B_p^h D_c^l s[k] & B_p^h C_c^l & A_p^h - B_p^h D_c^l\,(1-s[k])\, C_p^h \end{bmatrix}. \tag{31}$$

$$B = \begin{bmatrix} 0 \\ B_p^h \end{bmatrix},\ C = \begin{bmatrix} 0,\ C_p^h \end{bmatrix}. \tag{32}$$

The time-varying parameters are shown in (23), (28), and (29).

Proof: In the previous derivation, we showed that Fig. 3 and Fig. 4 are equivalent in the sense that all signals entail the same information. Successive substitution of the state update and subsystems output in Fig. 4 yields the system representation in (30)-(32).

Definition 6 [LPTV System]: [33] Recall that we have defined z as a one-step time-shift operator in Section II. A. Then, a discrete-time linear time-varying system G is linear periodically time-varying (LPTV) with period $\tau \in \mathbb{N}$ if it commutes with the delay operator $z^{-\tau}$, that is, $z^{-\tau}G = Gz^{-\tau}$.

Remark 7: From Definition 6 and Theorem 5, the system $J_F\left(A[k], B, C, 0\right)$ in (30) is an LPTV system with a constant period F [5], [28]. Recall that an LTI system can be regarded as a special case of an LPTV system.

IV. EXPERIMENTAL RESULTS AND DISCUSSION

In this section, the developed FILC method is applied to a CNC motion stage, and the results are compared with those of the SILC scheme, revealing the superior performance of FILC, which constitutes Contribution C3.

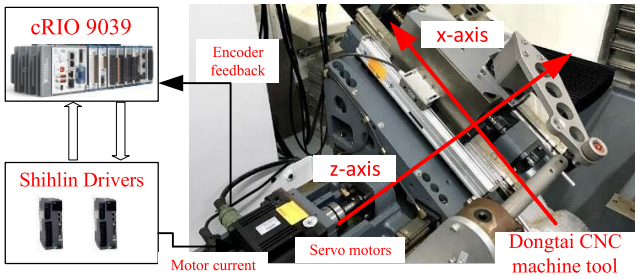

FIGURE 5. CNC machine tool motion stage.

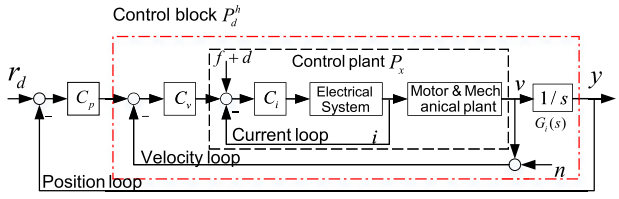

FIGURE 6. Servomotor cascaded three-loop structure, f denotes friction, d denotes process disturbance, and n denotes velocity measurement noise.

A. EXPERIMENTAL STAGE

The experimental X-Z motion stage shown in Fig. 5 comprises servo motors, ball screws, and the stage and is widely used in CNC machine tools. The pitches of the two axes are 10 mm (x-axis) and 12 mm (z-axis). Both motors are equipped with rotary encoders with a resolution of 52μrad/pulse.

The servomotor of each axis is independently controlled by a cascaded three-loop structure, as shown in Fig. 6, which includes an outermost position loop, a middle velocity loop, and an innermost current loop. Each loop has its own controller operating at different sampling rates and aims to make the corresponding closed-loop transfer function as close to identity as possible. Therefore, the servomotor control system in Fig. 6 is inherently a multirate system, with the highest sampling rate in the innermost loop.

In this paper, we consider the closed current loop as the plant, that is, P_x and P_z, which is within the dashed box in Fig. 6 and has the torque command and velocity as its input and output, respectively. Surrounding the plant are the velocity loop with a higher sampling rate $f^h = 4$ kHz and the position loop with a lower sampling rate $f^l = 1$ kHz. Thus, $F = 4$ in this paper.

The discrete-time transfer functions of the x-axis and z-axis are identified from fast-rate experimental data. The magnitude responses of the transfer functions on both axes are shown in Fig. 7.

$$P_x^h(z) = \frac{0.006382z^{-1} - 0.007674z^{-2} + 0.003835z^{-3}}{1 - 3.558z^{-1} + 4.925z^{-2} - 3.147z^{-3} + 0.781z^{-4}}. \tag{33}$$

$$P_z^h(z) = \frac{0.01674z^{-1} - 0.03231z^{-2} + 0.01616z^{-3}}{1 - 3.785z^{-1} + 5.402z^{-2} - 3.441z^{-3} + 0.8252z^{-4}}. \tag{34}$$

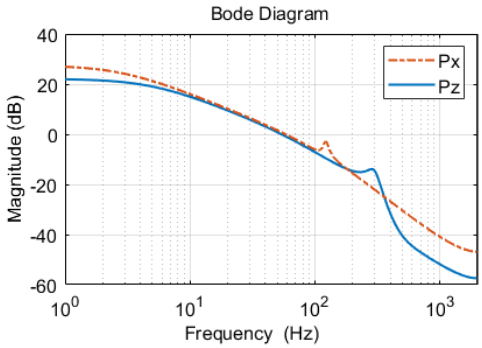

FIGURE 7. Frequency response of P_x^h and P_z^h.

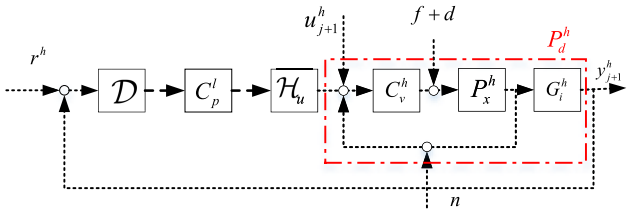

FIGURE 8. Implementation of FILC in the cascade control loops.

Because both axes have similar frequency responses below 100 Hz and are controlled independently, only the controller design procedure for the x-axis is detailed in this paper. Let $C_p^l(z)$ be the position controller, $C_v^h(z)$ be the velocity controller and $C_i(z)$ be a combination of the current controller and filter. The position controller is usually a PD structure with a lowpass filter in the derivative term, and the velocity controller is an PI structure. They are digitally implemented in the cRIO 9035 embedded system from National Instruments (NI). $C_p(z)$ and $C_v(z)$ are tuned by using the PID tuning toolbox in MATLAB, and $G_i^h(z)$ is a backward-type integrator. They are shown below.

$$C_p^l(z) = K_{pp} + K_{pd}\frac{1}{T_f + T^l z/(z-1)}. \tag{35}$$

$$C_v^h(z) = K_{vp} + K_{vi}\frac{T^h z}{z-1},\ G_i^h(z) = \frac{T^h z}{z-1}. \tag{36}$$

where $K_{vp} = 0.216, K_{vi} = 8.18, K_{pp} = 169, K_{pd} = 2.01, T_f = 1.01e^{-5}, T^h = 1/f^h, T^l = 1/f^l$.

Hence, the plant with respect to the position loop controller $C_p(z)$, i.e., the closed-loop system within the red dash-dot box in Fig. 6, can be characterized as P_d^h:

$$P_d^h(z) = \frac{C_v^h(z)P_x^h(z)}{1 + C_v^h(z)P_x^h(z)}G_i^h(z). \tag{37}$$

The nominal model in (33) and (34) includes one resonance mode at approximately 300 Hz in the x-axis and 120 Hz in the z-axis, and the position control loop yields a -3 dB bandwidth at 50 Hz and a gain margin of 20 dB.

Remark 8: Based on the results shown in Fig. 3, the implementation of FILC is shown in Fig. 8. The SILC in

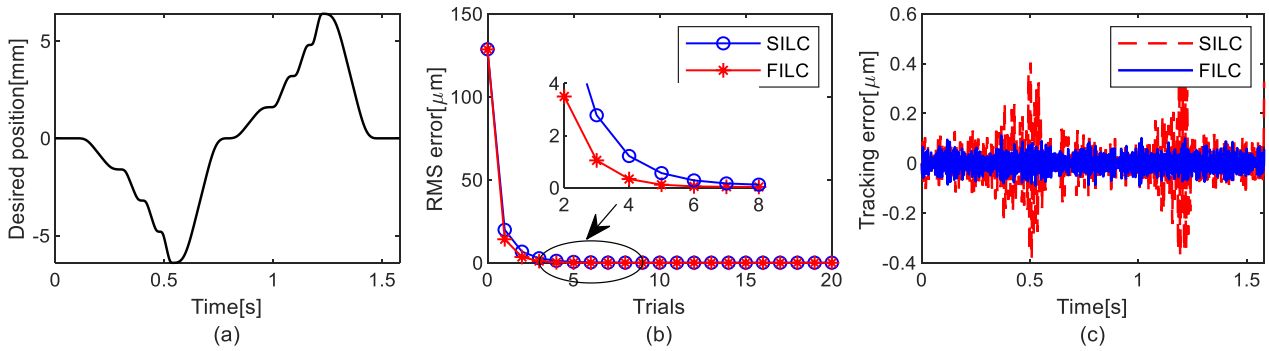

FIGURE 9. Simulation results. (a) Desired trajectory. (b) Convergence results of e_j^h. (c) The error comparison result of SILC and FILC after 10 trials ($j = 10$).

Fig. 2 is also implemented for comparison, where $P_d^l(z)$ can be obtained from $P_d^h(z)$ according to Lemma 3.

B. SIMULATION RESULTS

The effectiveness of the proposed FILC structure is verified by performing simulations on the ball-screw-driven stage. In the simulation, suppose that the simulation model is exact; hence, the weights (see (7)) are selected as $w_q = 10^6$, $w_r = 10^{-10}$, $w_s = 0.005$ for both SILC and FILC, with the aim of achieving fast convergence with high performance (discussed in Section II.B).

The measurement noise n and process disturbance d in Fig. 8 are added to the simulation, but the friction is assumed to have been perfectly compensated and is discarded ($f = 0$). d and n are modeled as Gaussian white noise with zero mean and variance $\sigma_n^2 = (0.5mm/s)^2$ and $\sigma_d^2 = (0.5A)^2$, respectively, according to the experimental measurements. Note that this kind of noise introduces a trial-varying disturbance, which cannot be compensated in the repetitive process through ILC, hence limiting the achievable performance. In addition, the error signal is measured with the high rate i.e., $f^h = 4$ kHz, for performance evaluation in the simulations and experiments.

The simulation results are shown in Fig.9. Fig.9(a) shows the desired trajectory, which combines a series of smoothed step references, and each step reference is planned using the S-curve velocity profile. This high acceleration step trajectory is suitable for testing the dynamic response of a motion system. The convergence result in Fig.9(b) shows that the transient of FILC is better than that of SILC. The root mean square (RMS) of error e^h for the first eight trials of FILC decreased twice as fast as that of SILC since FILC responds directly to e^h, while SILC responds to e^l. As e^h entails richer information than e^l, FILC can more effectively learn the tracking error and achieve faster convergence. Fig.9(c) shows the comparison of the resultant errors at the 10^{th} trial ($j = 10$) for SILC and FILC, which shows that FILC is superior to SILC. FILC learns the full error signal and significantly improves the performance compared with SILC.

This simulated case shows that SILC has inferior performance, and FILC achieves quick convergence of the error norm compared with SILC. The reason is that downsampling e^h causes a loss of high-frequency error components and slows down the learning process of the ILC. Next, the simulation results are validated with experiments in Section IV-C.

C. EXPERIMENTAL RESULTS

The FILC and SILC designed in the previous simulation are applied to the motion stage, as shown in Fig. 5. Contrary to the simulation case in Section V-B, the performance weights in (7) are chosen as $w_q = 10^6, w_r = 10^{-6}, w_s = 0.5$, considering the model mismatch in practice. Friction compensation is implemented using a look-up table based on prior experimental data, and the input of the look-up table is the reference velocity.

The reference shown in Fig.9(a) was also applied in the experiments. The experimental results are shown in Fig. 10. Similarly, Fig. 10(a) shows the convergence result of e_j^h for both SILC and FILC (in terms of RMS). Compared with the works in [29], the introduction of the parameterized model in the multirate frameworks accelerates the error convergence. Fig. 10(b) and Fig. 10(c) show the initial trial ($j = 0$) and the 10^{th} trial ($j = 10$) error results. In the 10^{th} trial, the RMS errors of e_j^h for SILC are 0.3808μm and 0.2038μm for FILC. These results show that the proposed FILC approach outperforms the SILC method, which is in line with the simulation results.

Furthermore, the fast Fourier transforms (FFT) of the above error signals at the 10^{th} trial ($j = 10$) at different sampling rates f^h and f^l are computed, and the results are depicted in Fig. 11. Fig. 11(a) shows that the dominant error component of the initial trial (without ILC) is below 50 Hz because the controller rejects the high-frequency components above 50 Hz at a cost of limited performance. Fig.11(b) and Fig.11(c) are the results of SILC and FILC, respectively, for the 10^{th} trial. Fig. 11(b, top) shows that SILC significantly reduces the error components below 100 Hz; however, some peaks are evident below 150 Hz. Comparing Fig. 11(b, top) with Fig. 11(b, bottom), we see that the peaks at 130 Hz

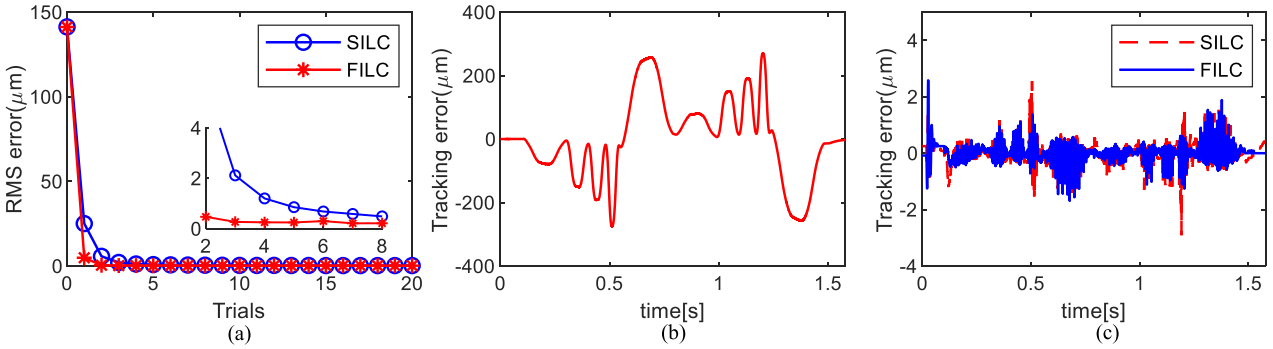

FIGURE 10. Experimental results (time domain). (a) Convergence results of e_j^h. (b) Initial trial error result (without ILC compensation). (c) The error comparison result of SILC and FILC after 10 trials ($j = 10$).

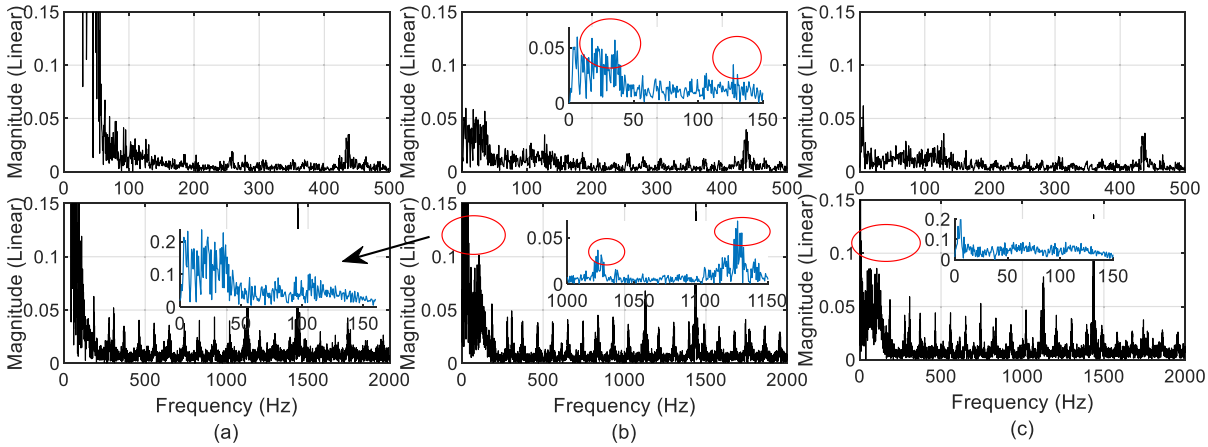

FIGURE 11. Experimental results (frequency domain). Top:e_j^l; bottom:e_j^h. (a) Initial trial (without ILC compensation). (b) After 10 trials ($j = 10$) with SILC. (c) After 10 trials ($j = 10$) with FILC.

and 30 Hz in Fig. 11(b, top) are due to the aliasing of the components at 1130 Hz and 1030 Hz in Fig. 11(b, bottom), respectively. In other words, the SILC system suffers from disturbance beyond the Nyquist frequency of the position control loop.

This problem can be overcome by FILC, as shown in Fig. 11(c, bottom), where the dominant low-frequency band under 150 Hz (in the close-up subfigure of Fig. 11 (c, bottom)) has a smaller magnitude than that in the close-up subfigure below 150 Hz of Fig. 11(b, bottom) because FILC responds directly to the fast-rate error signal e_j^h. Note that the high-frequency terms at 1030 Hz, 1130 Hz, 1500 Hz, etc. remain in FILC, since these terms may originate from even higher frequency components that cannot be attenuated by using u_j^h.

D. DISCUSSION

In summary, compared with SILC, FILC demonstrates the following advantages: i) Quick convergence is achieved, as shown in Fig. 9(b) and Fig. 10(a). ii) The accuracy is improved, as the RMS tracking error of FILC is approximately half of that of SILC for $j >= 8$ in experimental conditions (see Fig. 10(a)). iii) The aliased tracking errors are supressed, as shown in Fig. 11, because FILC can learn these error components beyond the Nyquist frequency of the feedback controller. The results also show that the proposed FILC method is applicable to large tasks.

V. CONCLUSION

In the automation industry, motion control loops usually operate at a low rate due to cost considerations. The single-rate design limits the achievable performance when ILC is applied owing to the loss of intersample information and beyond Nyquist frequency disturbances.

In this paper, a fast-update multirate ILC (FILC) framework is proposed to enhance the trajectory tracking performance of sampled-data control systems with multiple control loops and multirate structures. An efficient norm optimal technique based on a time-varying system model description was exploited to design the ILC update law in the FILC framework. However, such a model description is a primary challenge for multirate systems. A novel parametric linear periodic time-varying (LPTV) system model description is presented in this paper that converts the multirate system

into an equivalent single-rate system. Thus, the essential contribution of this paper is the FILC framework for performance enhancement that is not only effective but also implementable for large task applications by incorporating the norm optimal ILC method. Through simulations and experiments on a CNC motion stage, the proposed FILC method demonstrates its superiority in error reduction with a limited cost. Further research topic includes multiaxis simultaneous motion to realize complex machining paths in high-speed and high-precision applications.

APPENDIX A

Theorem A1 [Efficient Norm Optimal ILC]: Consider the performance criterion of Definition 1 and the LTV model in Section I (from $u_j[k]$ to $y_j[k]$) with the state space form as:

$$J(A[k], B[k], C[k], 0). \tag{A.1}$$

Then, the optimal $u_{j+1}[k]$ in (8) can be computed by the following steps:

Step 1: Solve the discrete Riccati equation backwards.

$$\begin{aligned} P[k] = A^T[k]P[k+1]A[k] - A^T[k]P[k+1]..\\ B[k](B^T[k] \times B[k] + \varphi)B^T[k]..\\ P[k+1]A[k] + C^T[k]w_qC[k]. \end{aligned} \tag{A.2}$$

where $P[N] = 0$ and

$$L[k] = (\varphi + B^T[k]P[k+1]B[k])^{-1}B^T[k]P[k+1]A[k]. \tag{A.3}$$

$$L_u[k] = (\varphi + B^T[k]P[k+1]B[k])^{-1}w_r. \tag{A.4}$$

$$L_g[k] = (\varphi + B^T[k]P[k+1]B[k])^{-1}B^T[k]. \tag{A.5}$$

$$\varphi = w_r + w_s. \tag{A.6}$$

Step 2:
Solve the vector difference backwards.

$$\begin{aligned} g_{j+1}[k] = (A^T[k] - K_g[k]B^T[k])g_{j+1}[k+1]\\ +C[k]w_qe_j[k] + K_g[k]w_su_j[k]. \end{aligned} \tag{A.7}$$

where $g_{j+1}[N] = 0$ and

$$\begin{aligned} K_g[k] = A^T[k]P[k+1](I + B[k]\varphi^{-1}\\ B^T[k]P[k+1])^{-1}B[k]\varphi^{-1}. \end{aligned} \tag{A.8}$$

Step 3:
Solve the optimal state as follows:

$$\begin{aligned} &\Delta x^*[k+1] = (I + B[k]\varphi^{-1}B^T[k]P[k+1])^{-1}(\\ &A\Delta x^*[k] - B[k]\varphi^{-1}w_ru_j[k] + B[k]B^T[k]g[k+1]). \end{aligned} \tag{A.9}$$

Step 4: Obtain the optimal ILC updates. Then,

$$\begin{aligned} u^*_{j+1}[k] = u_j[k] + \Delta u^*_{j+1}[k] = -L[k]\Delta x^*[k]\\ +(I - L_f[k])u_j[k] + L_g[k]g[k+1]. \end{aligned} \tag{A.10}$$

REFERENCES

[1] T. Chen and B. Francis, *Optimal Sampled-Data Control Systems*. London, U.K.: Springer, 1995.

[2] W. Ohnishi, T. Beauduin, and H. Fujimoto, "Preactuated multirate feedforward control for independent stable inversion of unstable intrinsic and discretization zeros," *IEEE/ASME Trans. Mechatronics*, vol. 24, no. 2, pp. 863–871, Apr. 2019, doi: 10.1109/TMECH.2019.2896237.

[3] W. Yan, C. K. Pang, and C. Du, "Disturbance observer-based multirate control for rejecting periodic disturbances to the Nyquist frequency and beyond," *Automatica*, vol. 82, pp. 49–58, Aug. 2017.

[4] Y. Gu and M. Tomizuka, "Multi-rate feedforward tracking control for plants with nonminimum phase discrete time models," *J. Dyn. Syst., Meas., Control, Trans. ASME*, vol. 123, no. 3, pp. 556–560, Sep. 2001, doi: 10.1115/1.1388013.

[5] J. van Zundert, W. Ohnishi, H. Fujimoto, and T. Oomen, "Improving intersample behavior in discrete-time system inversion: With application to LTI and LPTV systems," *IEEE/ASME Trans. Mechatronics*, vol. 25, no. 1, pp. 55–65, Feb. 2020, doi: 10.1109/TMECH.2019.2953829.

[6] L. Sun and M. Tomizuka, "Multirate adaptive disturbance suppression beyond Nyquist frequency," in *Proc. Int. Symp. Flexible Autom.* Kanazawa, Japan: The Institute of Systems, Control and Information Engineers, Jul. 2018, pp. 262–270.

[7] D. A. Bristow, M. Tharayil, and A. G. Alleyne, "A survey of iterative learning control," *IEEE Control Syst. Mag.*, vol. 26, no. 3, pp. 96–114, Jun. 2006, doi: 10.1109/MCS.2006.1636313.

[8] M. Norrlöf and S. Gunnarsson, "Time and frequency domain convergence properties in iterative learning control," *Int. J. Control*, vol. 75, no. 14, pp. 1114–1126, Nov. 2002, doi: 10.1080/00207170210159122.

[9] H.-S. Ahn, Y. Q. Chen, and K. L. Moore, "Iterative learning control: Brief survey and categorization," *IEEE Trans. Syst., Man, Cybern. C, Appl. Rev.*, vol. 37, no. 6, pp. 1099–1121, Nov. 2007, doi: 10.1109/TSMCC.2007.905759.

[10] Y. Wang, F. Gao, and F. J. Doyle, "Survey on iterative learning control, repetitive control, and run-to-run control," *J. Process Control*, vol. 19, no. 10, pp. 1589–1600, Dec. 2009, doi: 10.1016/j.jprocont.2009.09.006.

[11] D. Shen and G. Xiong, "Discrete-time stochastic iterative learning control: A brief survey," in *Proc. 10th World Congr. Intell. Control Autom.*, Beijing, China, Jul. 2012, pp. 2624–2629, doi: 10.1109/WCICA.2012.6358316.

[12] L. Wang, F. Liu, J. Yu, P. Li, R. Zhang, and F. Gao, "Iterative learning fault-tolerant control for injection molding processes against actuator faults," *J. Process Control*, vol. 59, pp. 59–72, Nov. 2017, doi: 10.1016/j.jprocont.2017.08.013.

[13] K. L. Barton and A. G. Alleyne, "A norm optimal approach to time-varying ILC with application to a multi-axis robotic testbed," *IEEE Trans. Control Syst. Technol.*, vol. 19, no. 1, pp. 166–180, Jan. 2011, doi: 10.1109/TCST.2010.2040476.

[14] J. D. Ratcliffe, P. L. Lewin, E. Rogers, J. J. Hatonen, and D. H. Owens, "Norm-optimal iterative learning control applied to gantry robots for automation applications," *IEEE Trans. Robot.*, vol. 22, no. 6, pp. 1303–1307, Dec. 2006, doi: 10.1109/TRO.2006.882927.

[15] T. Hsiao and P.-H. Huang, "Iterative learning control for trajectory tracking of robot manipulators," *Int. J. Autom. Smart Technol.*, vol. 7, no. 3, pp. 133–139, Sep. 2017, doi: 10.5875/ausmt.v7i3.1410.

[16] S. Mishra and M. Tomizuka, "Projection-based iterative learning control for wafer scanner systems," *IEEE/ASME Trans. Mechatronics*, vol. 14, no. 3, pp. 388–393, Jun. 2009, doi: 10.1109/TMECH.2008.2007302.

[17] Y. Chen, K. L. Moore, J. Yu, and T. Zhang, "Iterative learning control and repetitive control in hard disk drive industry—A tutorial," in *Proc. 45th IEEE Conf. Decis. Control*, San Diego, CA, USA, Dec. 2006, pp. 2338–2351.

[18] M.-S. Tsai, M.-T. Lin, and H.-T. Yau, "Development of command-based iterative learning control algorithm with consideration of friction, disturbance, and noise effects," *IEEE Trans. Control Syst. Technol.*, vol. 14, no. 3, pp. 511–518, May 2006, doi: 10.1109/TCST.2005.860521.

[19] T. Yang, N. Sun, and Y. Fang, "Neuroadaptive control for complicated underactuated systems with simultaneous output and velocity constraints exerted on both actuated and unactuated states," *IEEE Trans. Neural Netw. Learn. Syst.*, early access, Oct. 8, 2021, doi: 10.1109/TNNLS.2021.3115960.

[20] Y. Chen, B. Chu, and C. T. Freeman, "Generalized iterative learning control using successive projection: Algorithm, convergence, and experimental verification," *IEEE Trans. Control Syst. Technol.*, vol. 28, no. 6, pp. 2079–2091, Nov. 2020, doi: 10.1109/TCST.2019.2928505.

[21] Y. Chen, B. Chu, and C. T. Freeman, "Iterative learning control for robotic path following with trial-varying motion profiles," *IEEE/ASME Trans. Mechatronics*, early access, Apr. 22, 2022, doi: 10.1109/TMECH.2022.3164101.
[22] Y. Chen, B. Chu, and C. T. Freeman, "Iterative learning control for path-following tasks with performance optimization," *IEEE Trans. Control Syst. Technol.*, vol. 30, no. 1, pp. 234–246, Jan. 2022, doi: 10.1109/TCST.2021.3062223.
[23] L. Yang, Y. Li, D. Huang, J. Xia, and X. Zhou, "Spatial iterative learning control for robotic path learning," *IEEE Trans. Cybern.*, vol. 52, no. 7, pp. 5789–5798, Jul. 2022, doi: 10.1109/TCYB.2021.3138992.
[24] L. Blanken, G. Isil, S. Koekebakker, and T. Oomen, "Data-driven feedforward learning using non-causal rational basis functions: Application to an industrial flatbed printer," in *Proc. Annu. Amer. Control Conf. (ACC)*, Jun. 2018, pp. 6672–6677, doi: 10.23919/ACC.2018.8430777.
[25] U. Rosolia and F. Borrelli, "Learning model predictive control for iterative tasks. A data-driven control framework," *IEEE Trans. Autom. Control*, vol. 63, no. 7, pp. 1883–1896, Jul. 2018, doi: 10.1109/TAC.2017.2753460.
[26] B. Zhang, D. Wang, Y. Ye, Y. Wang, and K. Zhou, "Multirate iterative learning control schemes," in *Proc. 10th Int. Conf. Control, Autom., Robot. Vis.*, Hanoi, Vietnam, Dec. 2008, pp. 769–774, doi: 10.1109/ICARCV.2008.4795614.
[27] B. Zhang, Y. Ye, K. Zhou, and D. Wang, "Case studies of filtering techniques in multirate iterative learning control," *Control Eng. Pract.*, vol. 26, pp. 116–124, May 2014, doi: 10.1016/j.conengprac.2014.01.018.
[28] T. Oomen, J. van de Wijdeven, and O. Bosgra, "Suppressing intersample behavior in iterative learning control," *Automatica*, vol. 45, no. 4, pp. 981–988, Apr. 2009.
[29] W. Ohnishi, N. Strijbosch, and T. Oomen, "Multirate state tracking for improving intersample behavior in iterative learning control," in *Proc. IEEE Int. Conf. Mechatronics (ICM)*, Kashiwa, Japan, Mar. 2021, pp. 1–6, doi: 10.1109/ICM46511.2021.9385661.
[30] H. Liu and Y. Wang, "ERROR compensation system and method for numerical control (NC) machine tool based on iterative learning control," U.S. Patent 11 360 455 B1, Jun. 14, 2022. [Online]. Available: https://www.freepatentsonline.com/11360455.html
[31] T. D. Son, G. Pipeleers, and J. Swevers, "Robust monotonic convergent iterative learning control," *IEEE Trans. Automat. Control*, vol. 61, no. 4, pp. 1063–1068, Apr. 2016, doi: 10.1109/TAC.2015.2457785.
[32] J. van Zundert, J. Bolder, S. Koekebakker, and T. Oomen, "Resource-efficient ILC for LTI/LTV systems through LQ tracking and stable inversion: Enabling large feedforward tasks on a position-dependent printer," *Mechatronics*, vol. 38, pp. 76–90, Sep. 2016, doi: 10.1016/j.mechatronics.2016.07.001.
[33] J. van Zundert and T. Oomen, "LPTV loop-shaping with application to non-equidistantly sampled precision mechatronics," in *Proc. IEEE 15th Int. Workshop Adv. Motion Control (AMC)*, Tokyo, Japan, Mar. 2018, pp. 467–472, doi: 10.1109/AMC.2019.8371138.

YULIN WANG received the B.S.E. degree in mechanical engineering from Guangdong Ocean University and the M.S. degree in mechanical engineering from the South China University of Technology, Guangzhou, Guangdong, China, in 2013. He is currently pursuing the Ph.D. degree in electrical and control engineering with the National Yang Ming Chiao Tung University, Hsinchu, Taiwan.

Since 2013, he has been a Lecturer at the College of Mechanical Engineering, Guangdong Ocean University. His current research interests include the modeling and control of mechatronics systems, with application to manufacturing systems and robotic systems, with a specialization in learning control.

TESHENG HSIAO (Member, IEEE) received the B.S. and M.S. degrees in control engineering from the National Chiao Tung University, Taiwan, in 1995 and 1997, respectively, and the Ph.D. degree in mechanical engineering from the University of California, Berkeley, CA, USA, in 2005. He is currently an Associate Professor with the Department of Electrical and Computer Engineering, National Yang Ming Chiao Tung University, Taiwan. His research interests include advanced vehicle control systems, robot motion and compliance control, and CNC precision motion control.